JOURNAL OF FIRE SCIENCES

Original Research Article

Journal of Fire Sciences
1–19

DOI: 10.1177/07349041251400304
journals.sagepub.com/home/jfs
Sage

Reliability of fire indicators based on the damage differential principle in wildland fire investigation: A laboratory approach

Raphael Ogabi[1], Michael Gallagher[2], Nicholas Skowronski[3] and Albert Simeoni[1]

Abstract

Reliable interpretation of fire pattern indicators is essential for wildland fire origin investigations, yet experimental validation is scarce. Damage Differential in the context of this study refers to the measurable changes in combustible and noncombustible objects after fire exposure, enabling the comparison and contrast of fire-caused effects on different faces or zones of artifacts, as described in NWCG PMS 412 (2025, 2016, 2005) and NFPA 921. The principle was quantifiably applied using image analysis and statistical methods (ANOVA) to evaluate directional reliability under controlled wind and fuel conditions. Our approach aims to reduce subjective interpretation by linking observed damage to specific fire dynamics and environmental factors. This study presents laboratory-scale wind tunnel experiments evaluating the directional behavior of commonly used indicators. Statistical analysis using ANOVA revealed that wind speed, fuel load, and artifact orientation each had a significant influence on fire indicators ($p < 0.001$). Findings show that while indicators can yield reproducible directional cues, their reliability is bounded by specific interactions between fire intensity and airflow conditions. A complementary field-scale study is underway to evaluate fire patterns in operational settings, thereby strengthening the scientific basis for evidence-based wildland fire investigations.

Keywords

Wildland fires, NWCG, PMS 412, NFPA 921, forensic science, damage differential, fire pattern indicators, statistical analysis

Date received: 3 October 2025; accepted: 10 November 2025

[1]Department of Fire Protection Engineering, Worcester Polytechnic Institute, Worcester, MA, USA
[2]USDA Forest Service, Northern Research Station, New Lisbon, NJ, USA
[3]USDA Forest Service, WO Fire and Aviation Management, Morgantown, WV, USA

Corresponding author:
Raphael Ogabi, Department of Fire Protection Engineering, Worcester Polytechnic Institute, Worcester, MA 01609, USA.
Email: ogabiraphael@gmail.com

Introduction

Wildland and wildland-urban interface (WUI) fires continue to pose significant threats to life, property, and ecological systems, with increasing frequency and severity driven by climate change, fuel accumulation, and development pressures.[1,2] The 2018 Camp Fire in California exemplifies this growing risk which claimed 85 lives, destroying more than 19,000 structures, and causing an estimated $16.5 billion in damages. It remains the second deadliest and the second most economically destructive wildfire in US history, with the deadliest being the 2023 Lahaina Fire (115 deaths), surpassed only by the 2025 Los Angeles Palisades and Eaton Fires.[3,4]

Accurate determination of fire origin and cause remains foundational to both fire investigation and the pursuit of justice. Central to fire origin determination is the use of fire pattern indicator. A fire pattern indicator is a physical object or artifact that displays changes when affected by a fire. An overall fire pattern is derived from the accurate analysis of individual fire pattern indicators and shows the general fire progression.[2,5]

To interpret these indicators and infer fire progression and origin directionality, the fundamental principle of Damage Differential is applied. In this study, "damage differential" refers to the principle of comparing and contrasting the extent of fire-related change such as charring, loss of material, and sooting between different sides or areas of objects after fire exposure. This approach aligns with the guidance provided in various editions of the NWCG PMS 412 (2025, 2016, 2005) and NFPA 921, where damage differential serves as a fundamental method to interpret fire pattern indicators. By systematically assessing differences in fire effects, we aim to determine both the direction and relative intensity of fire exposure on artifacts, building on the evolving terminology and criteria detailed in these foundational standards. This research applies the damage differential principle quantitatively, providing objective metrics that complement established best practices in wildland fire investigation.[1,2,6]

These indicators are generally classified as macroscale (large single fire pattern indicator or overall patterns of indicators that are readily visible from a distance, for example, char angle, directional fall, protection effects, which can also be microscale) or microscale (fire pattern indicators that are generally only visible when viewed within close proximity, for example, sooting, spalling, and discoloration, which can also be macroscale) and are used to reconstruct fire progression back to its area of origin.[1,2]

Despite their widespread use, the reliability of these indicators has been called into question.[2,7] Traditional interpretation methods are largely qualitative and rely heavily on investigator experience, introducing subjectivity and raising concerns about reproducibility and legal defensibility.[1,7–9] Fire ignition origin and cause determination has evolved through foundational resources such as Bourhill's 1982 field guide, which provided early observational criteria for identifying wildfire direction indicators; the NFPA 921 Guide, first published in 1992, which established a systematic, science-based approach to fire and explosion investigations; and the NWCG's PMS 412, introduced in 2005.[5,10–15]

While the updated 2025 NWCG PMS 412 guide emphasizes a science-based, systematic methodology and provides expanded descriptions of fire pattern indicators, it also acknowledges that their reliability may vary with environmental conditions and requires continued validation.

This highlights a critical research gap: the need for quantitative, experimental studies that assess the repeatability and accuracy of FPIs under controlled and field conditions to strengthen their evidentiary value in wildfire investigations.[2]

This study evaluates fire indicators under controlled laboratory conditions, in contrast to previous and ongoing research that has examined composite patterns in field environments. The experimental design enables the measurement of the consistency of indicators produced by different artifacts through repeatability testing, providing a robust basis for assessing their reproducibility. Using the Damage Differential principle, the indicators are quantified to capture the extent and nature of fire effects under varying wind speeds, fuel loads, and material orientations. Furthermore, statistical analysis tools, including ANOVA, are applied to study the significance and reliability of the empirical data, ensuring that observed data are supported by quantitative evidence. Collectively, this approach strengthens the scientific foundation for interpreting fire patterns in a more realistic wildland fire investigation.

Materials and methods

This section outlines the materials selected to represent common fire scene artifacts, experimental setup, and the controlled conditions under which they were exposed to flame spread to generate the fire pattern indicators (fire effect).

Artifacts used

A set of supporting elements representing common structural and environmental materials were selected based on their relevance to fire scene investigations:

- Polyvinyl chloride (PVC) pipes—1.905 cm × 60.96 cm;
- Standard clay bricks—19.69 cm × 5.72 cm × 9.53 cm;
- Caribbean beach pebbles—2.54 cm to 7.62 cm;
- Clear glass beer bottles—330 mL capacity;
- Aluminum beverage cans—330 mL capacity;
- Oak fence posts—2.54 cm × 5.08 cm × 152.4 cm;
- Dry pitch pine cones—average length 4–7 cm; average diameter 3–5 cm.

Experimental set-up

Experiments were conducted in a laboratory-scale wind tunnel designed to simulate linear flame propagation over vegetative fuel beds (Figure 1). The test section of the tunnel measured 3.0 m in length and 1.0 m in width, with transparent acrylic sidewalls to facilitate observations. Airflow was generated using an axial fan system calibrated to deliver uniform wind speeds across the test bed.

Wind speeds were verified using a digital hot-wire anemometer with a ±0.05 m/s accuracy. The rates of spread (RoS) were consistent with wind-driven conditions, where winds during the fires tilted the flames. However, near-surface winds were likely lower than the recorded values, which may partly explain the observed spread behavior.

To contextualize our laboratory-derived RoS, we reference published field experiments using similar fuel types. Mueller et al.[17,18] reported RoS in pine-needle litter ranging between

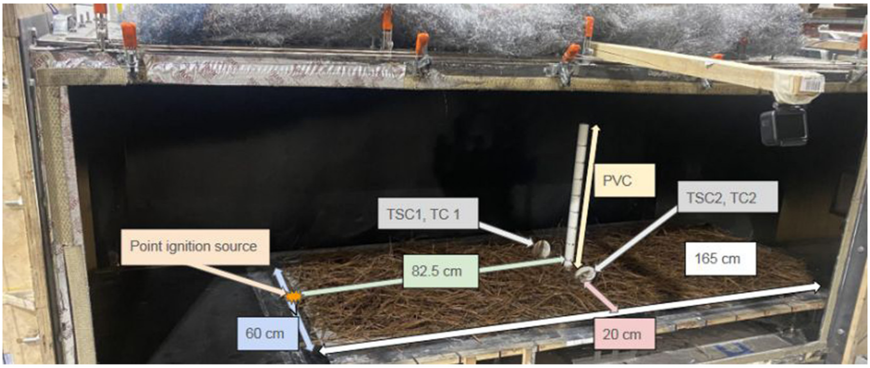

(a)

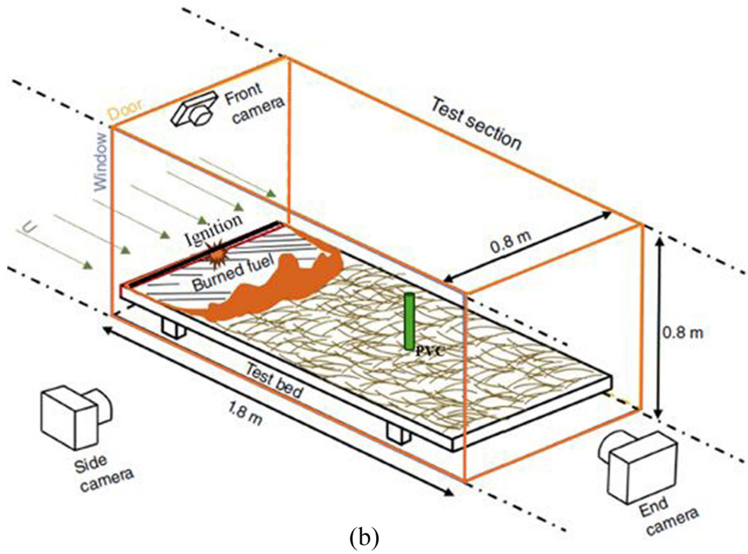

(b)

Figure 1. The experimental setup used for the laboratory tests. (a) Laboratory-scale wind tunnel used for the fire pattern generation by flame impingement. (b) Schematic diagram of the wind tunnel used showing the fuel bed configuration, artifact staged, ignition point, wind direction, and camera locations.[16]

0.2 and 5.0 cm s^{-1} under light, variable wind conditions, demonstrating that our lab values fall within the observed field range.

Thin skin calorimeter (TSC) and K-type thermocouples devices were used for the total heat flux measurement. In addition, video footage was captured using three GoPro cameras at 120 frames per second to provide visual coverage views (front, side, and rear) during fire progression.

Fuel bed preparation

The fuel bed was composed of uniformly dried pine needles (*Pinus rigida*, PR), the average fuel moisture content was 10.14% ± 0.64% (dry basis) for the respective trials. Moisture levels were determined for each experiment by oven-drying two randomly selected 15 g samples from the test bed at 60°C for 24 h, following the method of Schemel et al.[19,20] The pine needles were evenly distributed across the horizontal surface of the bed. This fuel type was selected due to its structural similarity to fine surface fuels commonly found in pine-dominated wildland environments.

Controlled conditions

A single point-source ignition was used (a representative of a more realistic wildland fire scenario) to initiate flame spread at the upwind end of the fuel bed A thin nickel-chromium wire (0.33 mm in diameter) was centrally positioned 82.5 cm from the staged artifact and heated using a high-voltage signal to ignite a few drops of methanol placed on it. The initial spread of the fire was generally elliptical, and the intensity increased as the fire progressed outward from the ignition point. The experiments were carried out under varying wind speed and fuel load conditions. The selected fuel loadings are representative of fine surface fuel beds, particularly pine litter.[21]

Data acquisition and measurement

Visual documentation of flame progression and artifact response was recorded using high-resolution cameras at three vantage points: a multi-angle camera setup was employed to capture fire behavior: the frontal view recorded flame–artifact interactions, the overhead view monitored spread dynamics and resulting surface patterns, while the rear view assessed the development of indicators on the back (leeward) side.

Indicators were identified and classified according to categories defined in the NWCG Guide to Wildland Fire Origin and Cause Determination (PMS 412 and NFPA 921 guides). The following fire pattern indicators were evaluated:

- Angle of deflection and height of deformation of PVC pipe (included as supplementary artifacts beyond those listed in the NWCG guide);
- Amount of sooting (bricks, rocks);
- Amount of staining (glass bottles, aluminum cans);
- Angle of char (wooden posts);
- White ash (pitch pine cones);
- Protection.

Data analysis

Data analysis was carried out to quantify material responses in terms of fire damage or surface scarring under controlled experimental conditions. A combination of image processing techniques and statistical tools was employed to ensure objective and reproducible evaluation.

Image processing. To enable a quantifiable and repeatable assessment of fire effects, adhering to the Damage Differential principle, a systematic image processing methodology was employed. This objectively measures and compares fire damage to deduce relative fire exposure intensity.

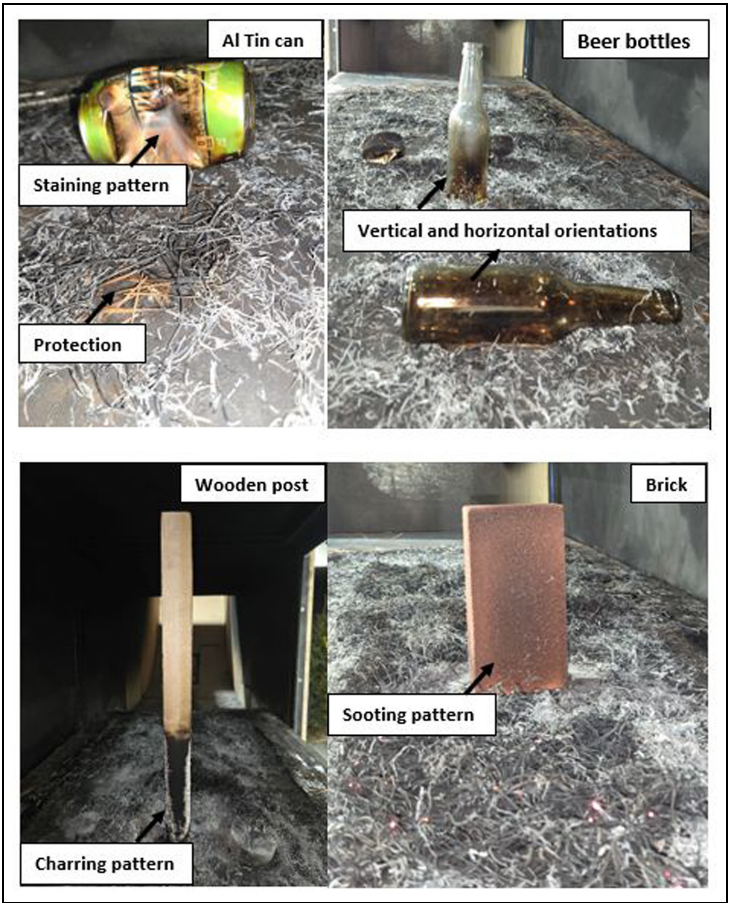

Figure 2. Fire pattern indicators generated on representative materials following exposure in a laboratory wind tunnel.

Digital image processing has been applied in fire forensics and smoke deposition studies to quantify post-fire surface effects. For instance, Riahi[22] used grayscale conversion, thresholding, and pixel intensity analysis to measure smoke residue on filters and walls, correlating optical density with gravimetric mass for forensic documentation. Similarly, Riahi and Beyler[23] quantified smoke patterns on vertical walls via photographic analysis, deriving optical density to validate thermophoretic models.

Riahi et al.[24] extended this to hot smoke layers using image-based optical measurements on glass filters for deposition rate prediction. For gypsum board damage, Gorbett et al.[6] applied adaptive thresholding and segmentation to identify lines of demarcation, enabling quantitative analysis of calcination depth and fire patterns.[23–25]

Building on these, this methodology adapts digital image processing to quantify directional fire effects on wildland artifacts in controlled wind tunnel conditions. Unlike prior foci on smoke mass or structural patterns (e.g. walls or gypsum), it measures proportional damaged area for directionality, and indicators such as soot scarring and staining relative to wind-driven exposure. Processing used two-dimensional photographs, quantifying damage on visible surfaces via high-resolution pre- and post-burn images. MATLAB scripts extracted consistent metrics across damage types.

Images were converted to grayscale, cropped to isolate regions of interest, normalized using pre-fire images to subtract lighting and reflections, and segmented via adaptive thresholding to identify fire-affected areas. Damaged area was computed in pixels and converted to cm^2 using calibrated scales from artifact dimensions in section "Artifacts used," enabling objective comparisons under varying wind and fuel loads.

Despite standardization of lighting, positioning, and calibration, uncertainties persist from variability in lighting, threshold sensitivity, pixel scaling, overlapping stains, reflections, and edge effects, potentially affecting segmentation accuracy. These were mitigated via normalization, repeated trials, and consistent algorithms, but should be considered in result interpretation. Overall, the method robustly quantifies relative fire damage differences in controlled settings.

Statistical analysis. To evaluate the sensitivity of fire pattern indicators to controlled variables, a two-way analysis of variance (ANOVA) was conducted. Depending on the indicator, the tested factors included fuel load, wind speed, and surface orientation (e.g. front vs back faces or alignment angle), as well as their interaction effects.

The ANOVA compares the variance between groups (e.g. different wind, fuel, or orientation conditions) to the variance within groups (random variability), producing an F-statistic, defined as the ratio of mean square between groups to mean square within groups (Supplemental Appendix A). Degrees of freedom were assigned to each factor (df1) and to the residual error (df2), and the corresponding p-value was derived from the F-distribution. A p-value less than 0.05 was considered statistically significant.[26]

This method ensures that observed trends are not due to chance, thus strengthening the individual assessment of the reliability of the fire indicators.

Results and discussion

This section presents the observed behavior and reliability of key fire pattern indicators across varying wind speeds and fuel loads. The indicators were assessed based on their directional consistency with the known fire origin and progression, as well as their expression across five experimental replicates per condition. In evaluating the reliability of a fire pattern indicator following flame impingement the study focuses on two fundamental aspects:

1. Repeatability (Precision): The extent to which the fire indicator is consistently reproduced under identical experimental conditions.
2. Responsiveness (Sensitivity): The degree to which the fire pattern varies in a measurable and meaningful way in response to controlled variables such as wind speed, fuel loading or orientation reflecting its sensitivity to changing fire dynamics. This was done using ANOVA to determine the statistical significance of each fire indicators.

In this study, Damage Differential is defined as the measurable change in combustible and noncombustible objects after fire exposure, quantified by comparing and contrasting fire effects (e.g. char depth, soot deposition, material loss, staining, or deformation) between opposing faces, zones, or orientations of an artifact to infer the direction and relative intensity of fire exposure. This definition is recognized in the 2025 NWCG PMS 412:

Individual-scale damage differential—the side-specific variation in fire effects on a single object, used to determine which face was exposed to the oncoming flame front for example, greater leeward charring or soot on the surface of the bricks as illustrated in the diagram below.

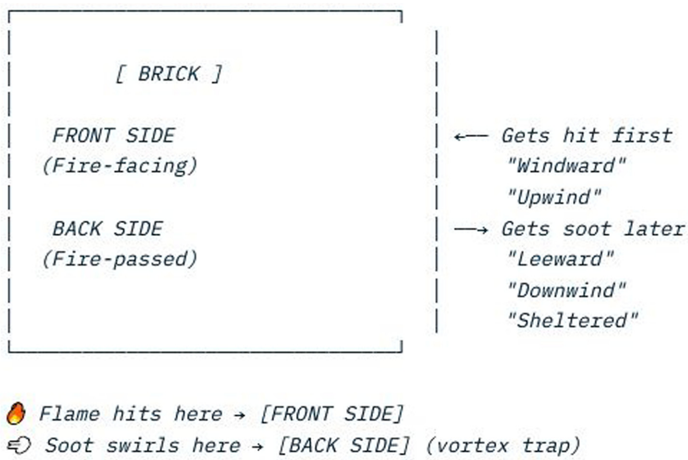

Degree of deflection and the height deformation

Polyvinyl chloride pipes were used because fire-pattern research[7,8] supports the use of man-made objects, including plastics, as valuable indicators in fire origin and progression analysis.

Figures 3 illustrates the representation the range of physical responses observed across varying wind speeds and fuel loads. These include distinct deflection patterns, typically away from the flame front and varying degrees of thermal deformation and melting. The visual evidence captured in these figures highlights the potential for PVC pipe to serve as a micro-scale fire pattern indicator under controlled conditions.

As shown in Figure 3, the angle of deflection observed in PVC pipe was influenced by both wind velocity and fuel loading. Given the wind conditions being analyzed, deflection angles consistently pointed back toward the origin of fire spread, supporting their use as directional indicators. However, at a higher wind speed, turbulence introduced notable variability in the deflection vectors.

This misalignment is likely caused by fluctuations in flame front behavior and the development of localized swirling air currents. The buoyancy-driven turbulence under no- or low-wind conditions produces natural plume instabilities that cause small angular oscillations, while wind-driven turbulence at higher velocities introduces shear, entrainment, and eddies that distort flame attachment and may amplify deflection away from the origin.

To assess the directional reliability of the PVC angle of deflection as a fire pattern indicator, each observed angle was compared to the known direction of fire origin (set at 0°). A conformity threshold of ±15° was defined, meaning any deflection angle falling within 345°

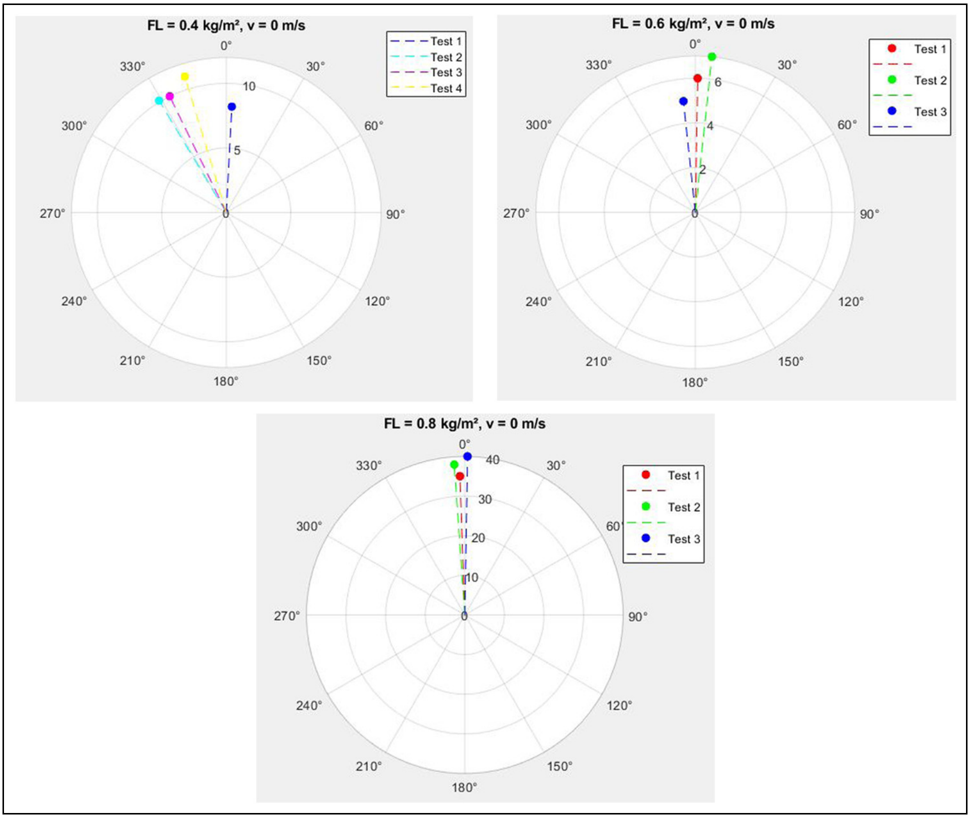

Figure 3. Directional alignment of PVC indicators at v = 0 m/s for fuel loads, FL of 0.4, 0.6, and 0.8 kg/m^2. Conformity threshold = ±15°.

to 15° was considered conforming. The ±15° tolerance was selected to balance practical measurement accuracy with natural variability in flame behavior: it reflects a narrow enough range to reliably identify alignment with the fire origin, while allowing for small deviations caused by turbulence from and measurement uncertainty.

For each test condition (combination of fuel load and wind speed), three replicates were evaluated. The number of angles that fell within the ±15° range was counted, and a conformity rate was calculated as:

$$Conformity\ rate = \frac{Number\ of\ conformity\ angles}{Total\ replicates}$$

This allowed a quantitative comparison of which test conditions produced repeatable and directionally accurate PVC angle responses as shown in Table 1.

Table 1 presents the conformity rate of PVC deflection angles relative to the fire origin at 0°, across varying wind speeds and fuel loads. Each bar represents a fuel load category, with height indicating the proportion of replicates falling within ±15° of the origin direction.

Table 1. PVC angle conformity summary (origin = 0°).

S/N	Fuel load (kg/m^2)	Wind speed (m/s)	Total replicates	Conforming count	Conformity rate	Mean angle
1	0.4	0.0	3	0	0.0	335.33
2	0.4	0.5	3	2	0.67	349.33
3	0.4	1.5	3	1	0.33	336.67
4	0.4	2.0	3	2	0.67	315.33
5	0.6	0.0	3	3	1.0	355.67
6	0.6	0.5	3	2	0.67	345.67
7	0.6	1.5	3	0	0.0	307.0
8	0.8	0.0	3	3	1.0	357.67
9	0.8	0.5	3	1	0.33	336.33
10	0.8	1.5	3	0	0.0	324.67
11	0.8	2.0	3	0	0.0	271.0

Conformity was highest under low-wind conditions (0.0–0.5 m/s) and declined with increasing wind speed, particularly at the lowest fuel load (0.4 kg/m^2).

After ignition, the flame plume spreads outward in all directions and sometimes latches irregularly onto the surface, which causes PVC angles to appear inconsistent in some conditions. As the fire develops into a head fire and the plume is bent flat by the wind, the PVC angles align more clearly with the direction of fire spread. Under low fuel load, the head fire remains weak and is more easily disrupted by shear, so conformity declines more steeply with wind; under higher loads, a deeper, hotter flame produces more coherent deflection even with moderate wind, though reliability still degrades when turbulence dominates. A two-way ANOVA was conducted to examine the effects of fuel load, wind speed, and their interaction on the angle of deflection.

Results showed that fuel load ($F = 1.06$, $p = 0.3144$), wind speed load ($F = 2.29$, $p = 0.1252$), or their interaction ($F = 1.16$, $p = 0.3576$) had a statistically significant effect on angle deflection (Supplemental Appendix B, Table 2a).

This suggests that PVC deflection angles may only be reliable under certain wind conditions, as seen in the conformity rate analysis. This fire effect is consistent with field evidence that indicator reliability varies with local fire conditions, so they must be interpreted in the context of overall fire dynamics.[7]

Bars represent the mean degraded length (cm) for each condition. Error bars denote the standard error of the mean (SE). The red bar at 2.0 m/s is absent because no valid measurements were obtained for that fuel load.

Deformation length is analyzed here as a continuous response to test conditions, not as a pass/fail directional metric. Figure 4 shows PVC deformation length, the melt length along the pipe as a continuous proxy for exposure intensity (distinct from the binary conformity used for deflection angles). Deformation was generally greater on the leeward side, increased with fuel load, and decreased with wind speed: the longest lengths occurred at 0.8 kg m^{-2} with 0.0 – 0.5 m s^{-1}, while the shortest occurred at higher wind and lower load. This pattern reflects longer flame residence and higher heat feedback at low wind/high load, versus flame flattening and entrainment at higher wind, which limit impingement and dilute the near-surface combustion zone. The deformation length showed strong statistical sensitivity to

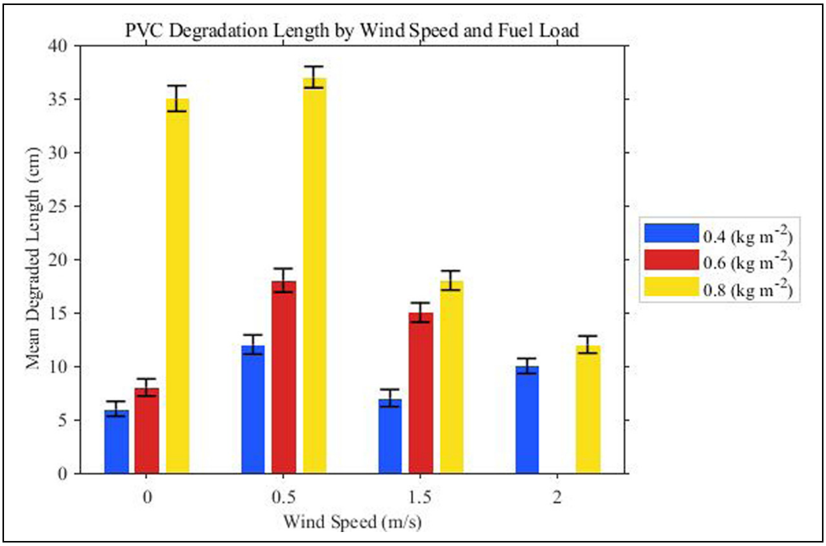

Figure 4. Mean PVC deformation height across wind speed and fuel load conditions (SE = ±0.95).

both fuel and wind parameters. ANOVA revealed highly significant main effects of fuel load ($F = 165.87$, $p < 0.001$, wind speed ($F = 15.83$, $p < 0.001$), and their interaction ($F = 27.23, p < 0.001$). This represents a Damage Differential in plastic deformation due to varying fire exposure. These results confirm that deformation length is a robust and responsive fire indicator (Supplemental Appendix B, Table 2b).

Amount of sooting

The results demonstrate distinct Damage Differential indicator in soot deposition on bricks and rocks, varying significantly with material type and wind conditions.

Figure 5(a) shows the area of soot deposit on the front and back faces of brick surfaces under varying fuel loads and wind speeds.

We restricted analysis to the windward (front) and leeward (back) faces; the lateral faces were excluded because edge recirculation and shadowing produced faint, inconsistent deposits and higher measurement uncertainty.

On brick surfaces, the back face generally exhibited higher soot accumulation under certain conditions. For instance, at a fuel load of 0.4 kg/m^2 with no wind (0 m/s), the back face-stained area was approximately 80 cm^2, compared to 75 cm^2 on the front face. This trend persisted with increased fuel load: at 0.8 kg/m^2, 0 m/s, the back face showed 76 cm^2 versus 72 cm^2 on the front. The effect became more pronounced under wind-driven conditions. At 0.8 kg/m^2 and 0.5 m/s, the back face registered 92 cm^2, while the front reached 76 cm^2, indicating a 21% increase, likely due to flame wrap and vortex-induced recirculation behind the object.

The results indicate that under wind-aided conditions, greater soot accumulation was observed on the back face, consistent with downstream entrainment and recirculation of combustion products.

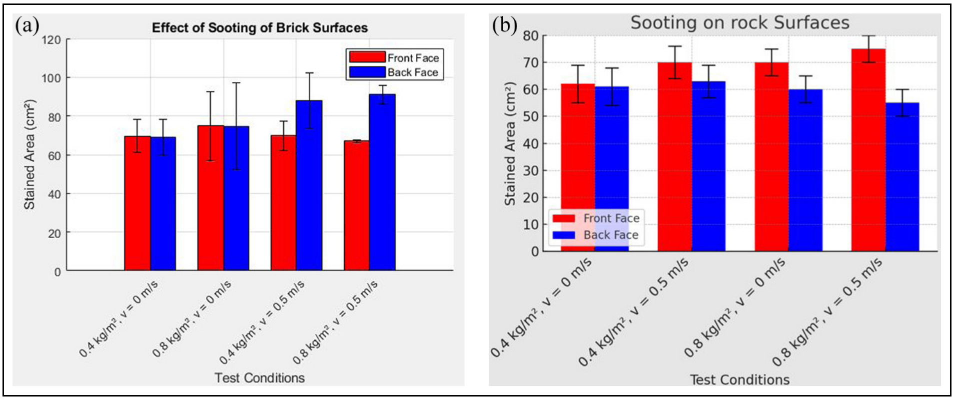

Figure 5. Soot deposition under varying conditions on the front and back surfaces of (a) brick, SE = ± 1.4 cm^2 and (b) rock, SE = ± 0.7 cm^2.

To better understand sooting behavior, we examined whether (1) the front or back face accumulates more soot, (2) wind speed influences the extent of sooting, and (3) wind affects the front and back faces differently that is, whether there's a combined (interaction) effect between face orientation and wind. These questions were addressed through ANOVA analysis, which revealed statistically significant effects of surface orientation ($p = 0.0365$) and wind speed ($p = 0.0205$) on the stained area. Fuel load had no significant effect ($p = 0.6139$), suggesting that within the tested range the ventilation-driven transport and deposition of smoke/soot governed the observed staining pattern more than differences in soot generation associated with fuel quantity (see Supplemental Appendix 2, Table 3). This supports the hypothesis that wind conditions play a critical role in directional sooting indicator.

Figure 5(b) presents the stained area measured on the front and back surfaces of rock artifacts under varying fuel loads and wind speeds.

In contrast, rock surfaces showed a different pattern, with the front face typically receiving more soot, especially under wind influence. At 0.4 kg/m^2 and 0.5 m/s, the front face recorded 73 cm^2, compared to 66 cm^2 on the back, yielding a 10.6% increase. Similarly, at 0.8 kg/m^2 and 0.5 m/s, front face sooting rose to 74 cm^2, while the back measured 62 cm^2, a 19.4% higher value. These results suggest that direct flame impingement dominated sooting behavior on rock surfaces, whereas brick surfaces were more influenced by rear-face vortex dynamics (flow obstruction effect), particularly under higher fuel loads and wind speeds.

We analyzed soot-stained area with a mixed-model ANOVA having face orientation (front/windward vs back/leeward) as a within-specimen factor and fuel load and wind speed as between-specimen factors (Supplemental Appendix B, Table 4).

Face orientation ($p < 0.001$), fuel load ($p < 0.001$), and wind speed ($p = 0.0025$) were significant; the fuel $\times$ wind interaction was significant ($p = 0.0243$), whereas face $\times$ wind was not ($p = 0.4020$). Here, the "face $\times$ wind" term represents the interaction between surface orientation (front/windward vs back/leeward) and wind speed, testing whether differences in soot deposition between faces varied as a function of wind velocity.

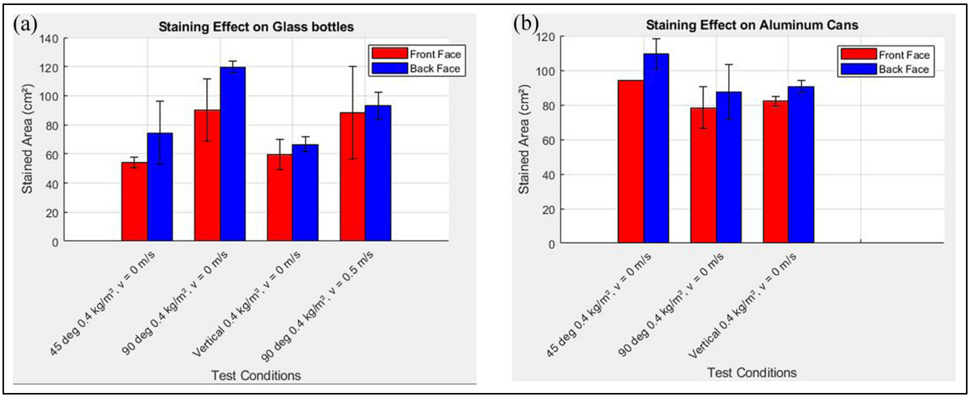

Figure 6. Staining indicator under varying orientations on the front and back surfaces of (a) beer bottles, SE = ±0.7 and (b) Al cans, SE = ±1.4.

These findings indicate that post-fire deposition patterns are governed not only by fire intensity and wind, but also by object geometry and associated flow dynamics, underscoring the need to account for shape effects in forensic fire analysis.

Future follow-up studies could vary brick orientation as well as the fuel type and load to further explore these dynamics.

Amount of staining

As illustrated in Figure 6(a), the highest soot accumulation occurred on the back face of bottles positioned at 90° with no wind, reaching approximately 120 cm^2, compared to 105 cm^2 on the front face. In contrast, vertical bottles exhibited lower deposition overall, with the front and back faces showing ~67 cm^2 and ~52 cm^2, respectively.

For bottles at 45° orientation, back faces also showed more staining (~90 cm^2) than front (~75 cm^2), reinforcing the idea of leeward accumulation due to recirculating combustion gases. At higher wind speeds (0.5 m/s), the sooting pattern shifted. For example, the back face of the horizontally placed bottles under wind exposure stained up to ~115 cm^2 compared to ~95 cm^2 for the front. These directional differences emphasize that even subtle changes in airflow and geometry can result in asymmetrical soot deposition. The statistically significant interaction between face and orientation further confirms that face exposure alone cannot explain staining behavior without accounting for bottle alignment.

ANOVA was conducted to investigate the influence of bottle face (front vs back), the orientation of the glass bottle relative to the flame direction (45°, 90°, vertical), and wind speed on the stained area of clear glass bottles. The ANOVA results ($F = 6.43$, $p = 0.022$ for Face; $F = 10.03$, $p = 0.0015$ for Orientation × Face interaction) indicate that both the surface orientation and its interaction with face type significantly affect soot deposition (see Supplemental Appendix 2, Table 5). This suggests the presence of directional sooting patterns influenced by airflow dynamics around cylindrical objects.

Protection indicator: A clean cut consisting of a patch of uncharred orange needles immediately windward of the brick marks a protected zone, while darker fused needles occur leeward. This indicator corroborates the flame attachment (called flame wrap in the guide)

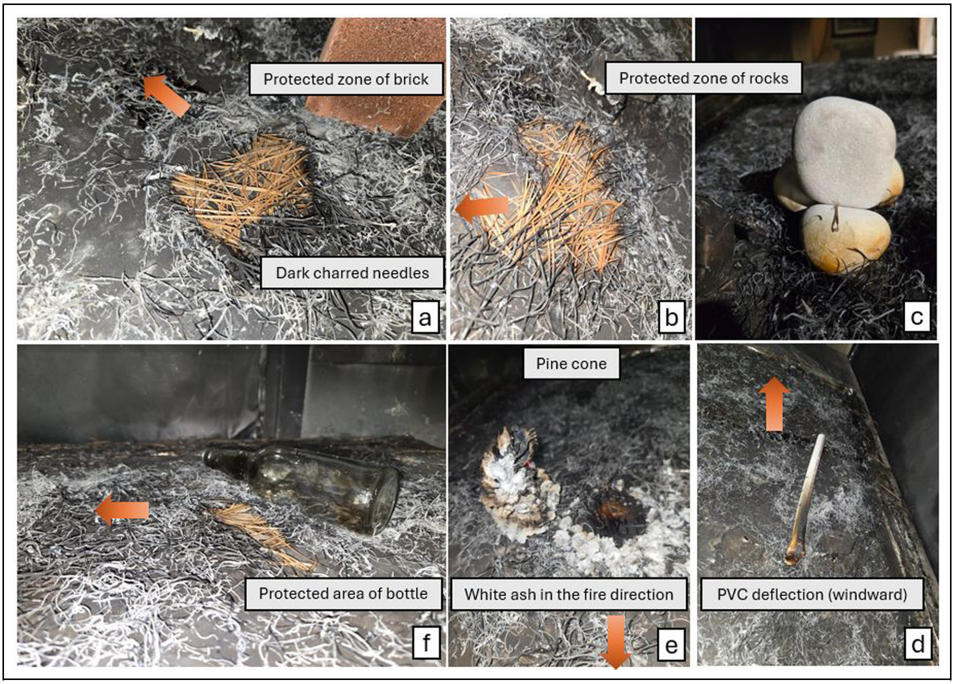

Figure 7. Protection zones and PVC deflection: cross-artifact indicators of fire-spread direction.

mechanism concentrating heat and soot on the brick's back face. In addition, a clean substrate "footprint" and lighter lee zone appear behind the stone, with greater ash/soot upwind.[2,5] This flow-shadow signature corroborates spread toward the protected wedge, produced by separation and reduced deposition in the lee (Figure 7).

Orientation: Upright = axis vertical; Horizontal φ = 90° = axis perpendicular fire-spread direction; Horizontal φ = 45° = axis at 45° to fire-spread direction. "Front"/"Back" denote windward/leeward halves relative to the spread vector.

Figure 6(b) presents the staining effect on aluminum can surfaces under varying orientations and wind speeds.

The results reveal that face orientation significantly affects soot deposition patterns, as supported by the ANOVA output ($F = 27.7$, $p = 0.0001$). Notably, back faces consistently accumulate more soot than front faces across all orientations and conditions.

From a fire dynamics perspective, this pattern aligns with the behavior of buoyant and wind-aided smoke movement around curved metallic surfaces.

At 45° and 90° orientations with no wind, the rear (leeward) surfaces trap and retain more soot due to flow separation and low-pressure recirculation zones formed downstream of the flame front. For example, under 45° with no wind, the back face exhibited a stained area above 110 cm^2, compared to approximately 95 cm^2 for the front face.

In contrast, vertical orientations with no wind show reduced sooting on both faces, suggesting diminished residence time of soot-laden gases due to reduced impingement angles. These observations reinforce the idea that surface orientation and geometry strongly influence a material's exposure to post-flame combustion products. However, ANOVA shows

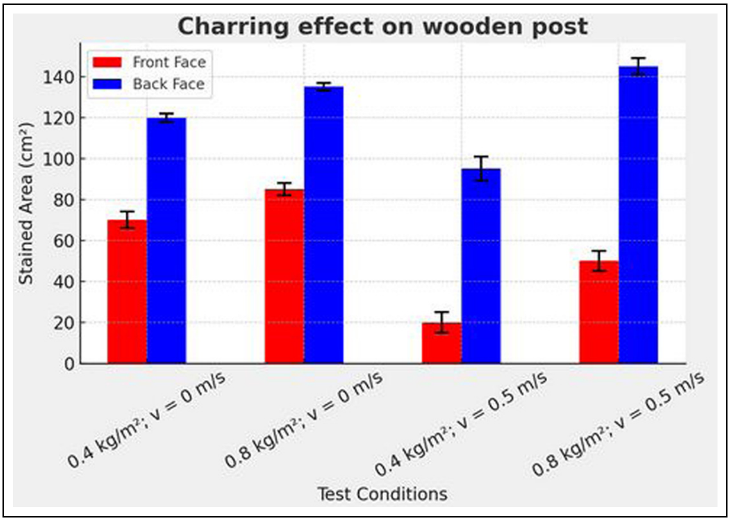

Figure 8. Directional alignment of fire pattern indicators under wind conditions for varying fuel loads (SE = $\pm$1.8).

that neither wind speed nor orientation alone had a significant effect ($p > 0.05$), likely due to minimal variation under the wind condition.

Interaction effects (e.g. Wind $\times$ Face and Orientation $\times$ Face) were also non-significant, indicating that the back-face dominance is consistent regardless of these secondary variables. These results underscore the reliability of back-face sooting as a potential fire pattern indicator for aluminum surfaces in low-wind scenarios (see Supplemental Appendix B, Table 6).

Angle of char

Char depth/area was measured on both the front and back faces to quantify the damage differential. The observed degree of charring of the wooden posts under varying wind speeds and fuel loads in Figure 8 highlights the influence of fire dynamics on charring. As illustrated in the graph, the back face consistently exhibited significantly larger stained areas compared to the front face across all conditions. This trend aligns with fire plume behavior, where wind drives flames and combustion products toward the leeward (back) face, enhancing charring behavior.

The charring results demonstrated a consistent trend of greater charred area on the back face of the wooden posts compared to the front face across all test conditions. At a fuel load of 0.4 kg/m^2 and no wind (0 m/s), the back face exhibited a stained area of 138.2 cm^2, which was 76% greater than the front face area of 78.5 cm^2. When the fuel load increased to 0.8 kg/m^2 under the same wind condition, the back face staining rose sharply to 203.6 cm^2, while the front face reached 110.2 cm^2, reflecting an 85% increase on the back face relative to the front. Under wind-driven conditions (0.5 m/s), the disparity became even more pronounced.

At 0.8 kg/m^2 fuel load and 0.5 m/s wind, the back face recorded the highest stained area at 247.3 cm^2, which was 136% higher than the front face value of 104.9 cm^2.

Table 2. Pine-cone ash content (mass loss, ML %).

Fuel ($kg{\cdot}m^{-2}$)	Wind ($m{\cdot}s^{-1}$)	ML% (T1)	ML% (T2)	ML% (T3)	n	Mean ± SD
0.4	0.0	79.6	65.8	74.5	3	73.3 ± 7.0
0.4	0.5	41.6	36.2	39.0	3	38.9 ± 2.7
0.8	0.0	73.8	89.9	82.0	3	81.9 ± 8.1
0.8	0.5	42.0	43.1	42.6	3	42.6 ± 0.6

The corresponding ANOVA results validate these observations. A statistically significant effect was found for surface face ($p = 0.0002$), confirming that orientation relative to the flame front influences charring. Wind speed had a moderate, though not statistically significant, influence ($p = 0.1058$), while the effect of fuel load was negligible within this data set (see Supplemental Appendix B, Table 7). Interactions between factors were not significant, suggesting that one effect counts and two are irrelevant.

Amount of white ash

White ash exposure takes place when the side of a combustible object facing the oncoming fire is exposed to higher intensity fire than the protected side, leading to more complete combustion on the exposed side and more white ash remains attached to the object. White ash exposure is directly related to fire intensity and fuel loading. In contrast, white ash deposits are formed when fine white ash particles are entrained in the convective plume and transported downwind until contacting a secondary object (combustible or noncombustible). Rocks and other smooth, noncombustible surfaces are particularly effective at capturing these deposits due to reduced adhesion on the source and enhanced downstream transport. Pine-cone ash indicator (mass-base) was calculated as the mass loss,

$$M_L = \frac{M_0 - M_r}{M_0} \times 100$$

Where M_0 is the pre-burn mass and M_r the post-burn residue. Table 2 shows an interesting trend: increasing wind from 0 to 0.5 $m{\cdot}s^{-1}$ lowers ML% at both fuel loads, and under calm conditions the higher load (0.8 $kg{\cdot}m^{-2}$) produces greater ML% than the lower load (0.4 $kg{\cdot}m^{-2}$).

Under no-wind, high-fuel conditions (0.8 kg/m^2, 0 m/s), ML% reached 81.8%, corresponding to extensive white ash attached to the cone scales, particularly on the windward (fire-facing) side—a classic white ash exposure pattern. This finding aligns with the PMS 412 description of white ash exposure as a fire pattern indicator.

This reflects prolonged flame attachment and complete oxidation. At 0.5 m/s, ML% dropped to ~39%–43% across both fuel loads, indicating shorter residence time and incomplete combustion due to enhanced ventilation, reducing attached ash.

Protection indicator: A charred dark patch of needles bordered by a crescent of white ash shows the flame came from the upwind side and moved downwind.[1,2] The narrow end of the charred area points the way the wind and fire moved as shown in Figure 7.

Notably, despite the prevalence of spalling in post-fire field assessments, no evidence of spalling was recorded in this study for either brick or pebble stone artifacts.

The absence of this effect may be due to the intensity of fire exposure levels, and the flame residence times under the controlled wind tunnel conditions.

While spalling can provide valuable directional and intensity cues in wildland fire investigations, its occurrence may require more extreme heating rates or mechanical stresses than those reproduced in this experimental setup. The absence of spalling in our trials does not diminish the significance of other observed and quantifiable indicators discussed above, which exhibited clear directional trends under the tested conditions.

Conclusion

This study evaluated the reliability of commonly cited fire indicators under controlled laboratory conditions using the principle of Damage Differential. Artifacts include PVC pipes, bricks, rocks, glass bottles, aluminum cans, wooden posts, and pine cones.

- **PVC pipes:** Deflection and deformation provided consistent directional cues under calm to moderate winds, but reliability declined at higher winds.
- **Bricks and rocks:** Contrasting soot deposition trends were observed, with bricks showing greater leeward staining and rocks more windward deposition, influenced by local flow/fire conditions.
- **Glass bottles and aluminum cans:** Orientation strongly influenced staining, with leeward consistently exhibiting greater area of soot deposition.
- **Wooden posts:** Wooden posts consistently demonstrated greater leeward charring.
- **Pine cones:** Produced quantifiable ash-loss indicators correlated with exposure intensity.

The findings underscore that while fire indicators can yield reproducible directional information, their reliability is context-dependent and shaped by interactions between fuel, wind, and object characteristics. These results support the need for quantitative frameworks to complement qualitative judgment in wildfire origin investigations, as emphasized in the updated NWCG PMS 412 and NFPA 921 guides. Importantly, the absence of spalling under the tested conditions highlights the influence of scale and exposure intensity, suggesting that certain indicators may only manifest under more severe or prolonged heating.

Recognizing that wildfire is a turbulent force, some fire pattern indicators may show directions opposite to the overall fire movement. However, the data indicate that even in such cases, the totality of all fire indicators, combined with fire behavior context, still reliably determines the true general progression of fire spread.

Overall, the work contributes to strengthening the evidentiary basis of wildland fire investigation by providing controlled experimental data that quantify indicator behavior and variability.

Future research should extend this approach to larger-scale and field conditions, where fuel heterogeneity, topography, and wind further affect the reliability of fire pattern indicators. By integrating laboratory and field insights, investigators can move toward a more scientifically robust, repeatable, and defensible methodology for origin determination in wildland fire contexts.

Acknowledgments

The authors acknowledge the collaboration and technical support provided by the USDA Forest Service, Northern Research Station (New Lisbon, NJ) and the USDA Forest Service, WO Fire and Aviation Management.

ORCID iD

Raphael Ogabi https://orcid.org/0000-0002-6817-9049

Funding

The authors disclosed receipt of the following financial support for the research, authorship, and/or publication of this article: This research was sponsored by the National Institute of Justice (Award No. NIJ-2020-17294).

Declaration of conflicting interests

The authors declared no potential conflicts of interest with respect to the research, authorship, and/or publication of this article.

Supplemental material

Supplemental material for this article is available online.

References

1. NWCG. Guide to wildland fire origin and cause determination. PMS 412. Boise, ID: National Wildfire Coordinating Group, 2016, https://www.nwcg.gov/publications/412 (accessed 13 July 2025).
2. NWCG. Guide to wildland fire origin and cause determination. PMS 412 (March 2025). Boise, ID: National Wildfire Coordinating Group, 2025, https://www.nwcg.gov/publications/412 (accessed 13 July 2025).
3. Maranghides A, Mell W, Hawks S, et al. *Preliminary data collected from the camp fire reconnaissance*. NIST technical note 2128, December. Gaithersburg, MD: National Institute of Standards and Technology, 2020.
4. CTIF. 911 down: 36 dead as Hawaiian residents jump in ocean for rescue when large wildfires burn both islands. International Association of Fire and Rescue Services (CTIF), 2023, https://www.ctif.org/news/911-down-36-dead-hawaiian-residents-jump-ocean-rescue-when-large-wildfires-burn-both-islands
5. Alexander M, Smith J and Thomas L. Global synthesis of quantification of fire behaviour characteristics in forests and shrublands: recent progress. *Curr Forest Rep* 2025; 11: 8.
6. Gorbett GE, Meacham BJ, Wood CB, et al. Use of damage in fire investigation: a review of fire patterns analysis, research and future direction. *Fire Sci Rev* 2015; 4: 4.
7. Simeoni A, Owens Z, Christiansen E, et al. A preliminary study of wildland fire pattern indicator reliability following an experimental fire. *J Fire Sci* 2017; 35(5): 359–378.
8. Parker K and Babrauskas V. Validation of NWCG wildfire directional indicators in test burns in coastal California. *Fire* 2024; 7(5): 5.
9. Danckwerts M. Physical evidence of fire and burn patterns. In: *Forensic fire analysis*, 1st ed. 2022, pp. 143–190. DOI: 10.1007/978-3-030-92847-3.
10. National Fire Protection Association. NFPA: 921: guide for fire explosion investigations. Quincy, MA: National Fire Protection Association, 2021.
11. Martin RA and Hamman ST. Ignition patterns influence fire severity and plant communities in Pacific Northwest, USA, Prairies. *Fire Ecol* 2016; 12(1): 88–102.
12. NWCG. *Wildfire origin & cause determination handbook (PMS 412-1)*. Boise, ID: National Wildfire Coordinating Group, 2005.
13. Nelson RM Jr. An effective wind speed for models of fire spread. *Int J Wildland Fire* 2002; 11(3–4): 153–161.
14. Abouali A, Viegas DX and Raposo JR. Analysis of the wind flow and fire spread dynamics over a sloped–ridgeline hill. *Combust Flame* 2021; 234: 111724.
15. Madrzykowski D and Fleischmann C. Fire pattern repeatability: a laboratory study on gypsum wallboard. *NIST technical report,* 2010, https://tsapps.nist.gov/publication/get_pdf.cfm?pub_id=906657
16. Singh A, Ziazi RM and Simeoni A. Intermittent fireline behaviour over porous vegetative media in different crossflow conditions. *Int J Wildland Fire* 2023; 32(4): 368–378.
17. Li Z, Li H, Yang Y, et al. Integrating earth observation data into the tri-environmental evaluation of the economic cost of natural disasters: a case study of 2025 LA wildfire. 2025, https://arxiv.org/abs/2505.01721
18. Mueller EV, Campbell-Lochrie Z, Walker-Ravena C, et al. Flame spread and combustion dynamics in pine litter under unsteady wind conditions. In: Viegas DX and

Ribeiro LM (eds) *Advances in forest fire research 2022*. Coimbra: University of Coimbra, 2022, pp. 1469–1476.
19. Sikkink PG, Lutes DE and Keane RE. *Field guide for identifying fuel loading models*. General technical report RMRS-GTR-225. Fort Collins, CO: U.S. Department of Agriculture, Forest Service, Rocky Mountain Research Station, 2009, https://www.fs.usda.gov/rm/pubs/rmrs_gtr225
20. Schemel CF, Simeoni A, Biteau H, et al. A calorimetric study of wildland fuels. *Exp Therm Fluid Sci* 2008; 32: 1381–1389.
21. Bowman DMJS, Haverkamp C, Rann KD, et al. Differential demographic filtering by surface fires: How fuel type and fuel load affect sapling mortality of an obligate seeder savanna tree. *J Ecology* 2017; 105(4): 1113–1124.
22. Riahi S. *Development of tools for smoke residue and deposition analysis*, Final report, NIJ award no. 2007-DN-BX-K236. U.S. Department of Justice, Office of Justice Programs, National Institute of Justice 2012, https://www.ojp.gov/pdffiles1/nij/grants/238725.pdf
23. Riahi S and Beyler C. Measurement and prediction of smoke deposition from a fire against a wall. *Fire Safe Sci* 2011; 10: 641–654.
24. Riahi S, Beyler CL and Hartman J. Wall smoke deposition from a hot smoke layer. *Fire Technol* 2013; 49(2): 395–409.
25. Hasnain M, Sezer H and Kozhumal SP. Predicting thermal response of gypsum board under various heat flux configurations: a three-dimensional mathematical model. *SSRN Electr J* 2024. https://papers.ssrn.com/sol3/papers.cfm?abstract_id=4926085
26. Otsu N. A threshold selection method from gray-level histograms. *IEEE T Syst Man Cybernet* 1979; 9(1): 62–66.

Author biographies

Raphael Ogabi is a Postdoctoral Research Fellow in the Department of Fire Protection Engineering at Worcester Polytechnic Institute (WPI), where he is currently investigating wildland fire investigations through field and lab-scale laboratory experiments. He earned his PhD in Energy from the National Institute & School of Applied Sciences (INSA CVL) in France. Previously, he served as a Research Officer at the National Research Institute for Chemical Technology in Nigeria, focusing on advanced natural fiber and polymer composites.

Michael Gallagher is a Research Ecologist for the US Forest Service Northern Research Station. Gallagher's research primarily focuses on understanding the dynamics of wildland fire behavior and spread and the effects of fire on forest vegetation. Much of Gallagher's work examines these themes from the perspective of prescribed fire and involves highly instrumented fireline experiments and the remote sensing of vegetation with lidar and multi-spectral sensors.

Nicholas Skowronski began his career as a Forester and Prescribed Burn Manager at Joint Base Dix-McGuire-Lakehurst. After earning his PhD at Rutgers University, he became a Research Forester with the USDA Forest Service Northern Research Station, specializing in remote sensing of 3D fuels, prescribed fire, and fire behavior. He has served as the PI of the North Atlantic Fire Science Exchange, on the Northeastern Regional Cohesive Strategy Committee, and on the Integrated Research Management Team. Most recently, he was the Project Leader of the USDA Forest Service's Northern Research Station's Fire Research Work Unit.

Albert Simeoni is a Professor and the Department Head of Fire Protection Engineering at Worcester Polytechnic Institute. He is an expert in wildland fire and fire science. He has experience in developing experimental, analytical, and numerical techniques to better understand fire dynamics and to predict fire and wildland fire behavior and impact.